Arabian Journal of Chemistry (2022) **15**, 103735

King Saud University

Arabian Journal of Chemistry

www.ksu.edu.sa
www.sciencedirect.com

ORIGINAL ARTICLE

An insight to catalytic synergic effect of Pd-MoS_2 nanorods for highly efficient hydrogen evolution reaction

Fozia Sultana [a], Muhammad Mushtaq [b], Jiahui Wang [c], Khaled Althubeiti [d], Abid Zaman [e], Aisha Kalsoom Rais [f], Asad Ali [g], Qing Yang [h,*]

[a] *Hefei National Laboratory of Physical Sciences at the Microscale (HFNL), Department of Chemistry, Laboratory of Nanomaterial's for Energy Conversion (LNEC), University of Science and Technology China, Hefei 230026, Anhui, PR China*
[b] *School of Material Science and Engineering, Beijing University of Technology, Beijing, PR China*
[c] *Hefei National Laboratory of Physical Sciences at the Microscale (HFNL), Department of Chemistry, Laboratory of Nanomaterial's for Energy Conversion (LNEC), University of Science and Technology China, Hefei 230026, Anhui, PR China*
[d] *Department of Chemistry, College of Science, Taif University, P.O. Box 11099, Taif 21944, Saudi Arabia*
[e] *Department of Physics, Riphah International University, Islamabad 44000, Pakistan*
[f] *Department of Chemistry, Abdul Wali Khan University, Mardan, Pakistan*
[g] *Department of Physics, Riphah International University, Islamabad 44000, Pakistan*
[h] *Hefei National Laboratory of Physical Sciences at the Microscale (HFNL), Department of Chemistry, Laboratory of Nanomaterial's for Energy Conversion (LNEC), University of Science and Technology China, Hefei 230026, Anhui, PR China*

Received 8 December 2021; accepted 24 January 2022
Available online 01 February 2022

KEYWORDS

Transition metal dichalcognides;
Catalytic hydrogen production;
Intrinsic activity;
Electrical conductivity;
Stability;
Solvothermal

Abstract The electrocatalytic hydrogen evolution reaction (HER) is a sustainable energy production route using green chemistry. Transition metal dichalcogenides' application in catalytic hydrogen production is limited due to a lack of solutions that simultaneously address intrinsic activity, increased surface area, electrical conductivity, and stability problems. Herein we address these issues simultaneously by modifying the electronic structure of molybdenum disulfide (MoS_2) nanorods using a low content of Pd (1 wt% and 2 wt%) dopant via a facile colloidal solvothermal route. The resulting MoS_2 nanorods doped with (1 and 2 wt%) palladium demonstrate current density of 100 mA/cm^2 at quit lower over-potentials of 137 mV and 119 mV than 273 mV for pure MoS_2

* Corresponding author.
E-mail addresses: fsultana@mail.ustc.edu.cn (F. Sultana), qyoung@ustc.edu.cn (Q. Yang).
Peer review under responsibility of King Saud University.

Production and hosting by Elsevier

https://doi.org/10.1016/j.arabjc.2022.103735
1878-5352 © 2022 The Authors. Published by Elsevier B.V. on behalf of King Saud University.
This is an open access article under the CC BY-NC-ND license (http://creativecommons.org/licenses/by-nc-nd/4.0/).

nanorods, accompanied by high stability. This research proposes a strategy for designing high-performance HER electrocatalysts that work in acidic medium. In addition, the Tafel slop calculated for MoS_2 is 112 mV/dec whereas for 1 and 2 wt% Pd-MoS_2, the Tafel slopes are 70 mV/dec and 46 mV/dec.

© 2022 The Authors. Published by Elsevier B.V. on behalf of King Saud University. This is an open access article under the CC BY-NC-ND license (http://creativecommons.org/licenses/by-nc-nd/4.0/).

1. Introduction

In the current economic scenario, we require more and more efficient technologies in every field due to increasing energy demand. The current high reliance on non-renewable fossil fuels (which are rapidly becoming unsustainable) has diverted the attention quickly and more deeply than in the past. As a result, scientists are putting out every effort to find a sustainable, renewable, and clean energy source in order to address energy concerns (Liling et al., 2020; Liling et al., 2019). The electrocatalytic hydrogen evolution process (HER: $2H^+ + 2e^- \rightarrow H_2$), which is critical for producing clean hydrogen energy, is one such clean energy generating phenomena (Jingying et al., 2020; Zexing et al., 2012). The lack of a cost-effective alternative for Pt has hindered the scale-up of hydrogen electrochemical generation for decades; comparable catalytic compounds are largely confined either by low catalytic performance or a finite lifespan (Zexing et al., 2021; Seh et al., 2017; Yang, 2016). As a result, low-cost, high-stability, and high-natural-abundance catalysts are required, as well as catalysts that would not become obsolete and will not obstruct HER implementation. Until recently, Pt/C was indeed the gold standard catalyst for hydrogen production (Ma, 2014). Recent research suggests that Mo based materials such as MoO_2 could be a promising non-noble-metal electrocatalyst for HER (Baohua et al., 2017). MoS_2 has been considered as particularly favorable for hydrogen evolution reaction (HER) since the activity of its metallic edges (GH = 0.06 eV) was theoretically anticipated by Norskv and co-workers, and later experimentally confirmed by Jaramillo and co-workers (Hinnemann, 2005; Jaramillo, 2007). The following are the main governing concepts for optimizing MoS_2 catalytic efficiency: 1. increase the density of atomically under-coordinated absorption sites in the trigonal prismatic phase (2H) MoS_2 by revealing edge sites or introducing in-plane sulfur vacancies (SVs) (Karunadasa, 2012; Kibsgaard et al., 2012; Tsai, 2017). Though, unleashing the inherently high activity is restrained by the semi-conducting property of 2H-MoS_2, where the charge transfer efficacy is restricted by an insufficiency of electrons at the chemical interface (Voiry, 2016; Li, 2015). Secondly, switching the MoS_2 phase from 2H to 1T, which is more conductive and thus more catalytically active (Kan, 2014; Lukowski, 2013). The active sites in 1T–MoS_2 are the S atoms in the basal plane; however, despite the substantially increased site density, these S sites have less acceptable hydrogen adsorption properties (GH = 0.17 eV) (Peng et al., 2021). Aside from these issues with 2H-MoS_2 and 1T–MoS_2, one big challenge with both of these substances have poor stability, since defective 2H-MoS_2 has a high sulfur leaching rate and 1T–MoS_2 is intrinsically metastable (Longfei and Jan 2021; Geng, 2016). MoS_2 appears to be widely applicable to the HER only when the electrical conductivity, site density, inherent activity, and stability concerns are all addressed at the same time. Owing to lower hydrogen adsorption energy of Molybdenum disulfide (MoS_2) compared to noble metals (among which Pt is one), indicating that MoS_2-based materials have a lot of potential as a replacement for Pt in the HER (Yan et al., 2014; Yipeng et al., 2019). The catalytic efficiency of MoS_2 could be improved even further by doping and/or substituting heteroatoms to lower the energy of hydrogen adsorption and modify the orbital structure of the valence and conduction bands, according to theoretical research (Zheng et al., 2015; Zexing et al., 2020). According to current study, doping MoS_2 with palladium (Pd) or transition metals like zinc (Zn) has been shown to boost HER activity (Song et al., 2021; Wu et al., 2019). Since it is commonly known, Pd and Mo have similar atomic radii. Therefore, we chose the element Pd as a dopant atom to examine its effects on MoS_2 based on the aforementioned concepts (see Table 1 and 2).

With the aforementioned background, this project aimed to synthesize Pd-MoS_2 nanorods (1&2 wt%) using one-pot solvothermal approach and the subsequent optimized electrochemical activity of Pd-MoS_2 for hydrogen evolution reaction.

2. Experimental section

The detail of materials used and fabrication of pure MoS_2 nanorods and Pd doped MoS_2 is described in detail below.

2.1. Materials

This experiment employed only analytical-grade chemical reagents. Molybdenum (VI) dioxide bis (acetylacetonate) [MoO_2 $(acac)_2$] and oleylamine (OAm, 70%) were purchased from Sigma-Aldrich. Dibenzyl disulfide [$(PhCH_2)_2Se_2$, 95%] was purchased from Alfa Aesar. Absolute ethanol and toluene were obtained from Sinopharm Chemical Reagent Ltd. All chemicals were used in the experiments without further purification.

2.2. Preparation of MoS_2 nanorods

In a typical synthesis, 0.5 mmol of Molybdenum (VI) dioxide bis (acetylacetonate) [MoO_2 $(acac)_2$] and 0.5 mmol Dibenzyl

Table 1 Average crystallite size (D) of MoS_2 nanostructures.

Composition	Average Crystallite Size "D" (nm)
Pure MoS_2	78.719
Pd-MoS_2-1 wt%	124.747
Pd-MoS_2-2 wt%	453.116

Table 2 HER activity comparison table showing the current density (mA/cm2) with overpotential (mV).

Catalyst	Electrolytes	Overpotential (mv vs.RHE) @100 mA/cm^2	reference
2 wt%Pd-MoS_2	0.5 M H_2SO_4	119	This work
Se-MoS_2/$Co_{0.2}Ni_{0.8}Se_2$	Universal pH	122	2
Col-Fel-B	1 M KOH	355	4
MoP@PC	0.5 M H_2SO_4	> 200	7
MoS_2NFs/rGO	0.5 M H_2SO_4	> 400	8
MoS_2-40	0.5 M H_2SO_4	> 200	9
1 T- MoS_2	0.5 M H_2SO_4	> 200	18
M- MoS_2	0.5 M H_2SO_4	> 300	19
N-WS_2/Ni_3FeN	1 M KOH	140	37
MoS_2/rGO/NiS-5	1 M KOH	212	36

disulfide [$(PhCH_2)_2S_2$] were dispersed in 10 mL of olylamine (OAm) using ultra-sonication for 30 min. After mixing well, 0.05 mg of Borane *tert*-butylamine (BTB) was added to the mixture of MoO_2 $(acac)_2$ and $(PhCH_2)_2S_2$ then ultrasonicate further for 10 min. The above-mentioned mixture was autoclaved for 12 h at 280 °C in a 50 mL Teflon-lined autoclave. The as-obtained product was centrifuged at 7000 rpm and washed with toluene 6 times before being dried in a vacuum oven at 70 °C for 3 h.

2.3. Preparation of Pd-MoS_2 nanorods

The synthesis technique for Pd-MoS_2 is the same as for MoS_2, with the exception that Pd $(acac)_2$ solution (1 wt% Pd in OAM) was used as per the specified MoS_2: Pd mass ratio. Similarly, another sample was prepared by adding 2 wt% Pd solution into the mixture of MoO_2 $(acac)_2$ and $(PhCH_2)_2S_2$.

3. Characterizations

3.1. Physical characterization

The as-obtained products were characterized using variety of techniques. A Philips X'pert PRO X-ray diffractometer with Cu K, λ = 1.54182 Å, a JSM-6700F, and a Hitachi H-7650 for SEM and TEM, correspondingly, were used to investigate the structure and surface morphology of the MoS_2 nanorods and Pd-MoS_2 (1 wt% and 2 wt%). The elemental composition and oxidation number of the composite elements were investigated using an X-ray photoelectron spectroscopy (XPS) VGESCA-LAB MKII X-ray photoelectron spectrometer with Mg as the excitation source. At ambient temperature, a JYLABRAM-HR Confocal Laser Micro-Raman spectrometer was used to examine the Raman spectra using a 514.5 nm argon laser.

3.2. Electrochemical measurements

Electrochemical measurements were performed in a three-electreode system on a CHI660E electrochemical workstation, using an Ag/AgCl (in saturated KCl sulution) electrode as the reference electrode and a graphite rod as the counter electrode. The following is how the working electrodes were managed to make: To begin, 5 mg of annealed catalyst (at 350 °C for 2 h in an inert environment) was dispersed in 1 mL of ethanol, and 40 μL of catalyst ink was drop-cast onto carbon paper (0.5 $\times 0.5 = 0.25$ cm^2), then dried in a 70 °C oven. The linear sweep voltammetry (LSV) curves were obtained from 0 to −0.8 V vs Ag/AgCl electrode in 0.5 M H_2SO_4 solution at a scan rate of 5 mV/S and the cyclic voltammetry (CV) measurements were tested under the same condition except the scan rate was 50 mV/s. Electrochemical impedance spectroscopic (EIS) tests were taken at potential −0.35 V at frequency ranging from 100 kHz to 0.1 Hz. For stability purpose, samples were continuously cycled for 1000 and 3000 cycles. Electrochemical active surface area (ECSA) was estimated by calculating Cdl (ΔJ vs different scan rates) in non-faradic potential range 0.33–0.43 V.

4. Result and discussion

The crystallinity and phase study of pure MoS_2 and Pd doped MoS_2 nanorods (1 wt% & 2 wt%) were demonstrated using XRD technique. Each 1 wt% Pd-MoS_2 and 2 wt% Pd-MoS_2 have a set of distinctive peaks at 40.7°,46.6°, and 68.1°, which correspond to the (1 1 1), (2 0 0), and (2 2 0) planes of the conventional fcc (face-centered-cubic) Pd crystalline structure, respectively (card # 03-065-6174) (Santra et al., 2013). In addition to the peaks for Pd, other peaks in the XRD pattern of Pd-MoS_2 that are simultaneously indexed to MoS_2 (0 0 2), (1 0 0), (1 0 3), and (1 1 2) demonstrate the effective doping of Pd on MoS_2 (card # 01-075-1539). Moreover, the XRD pattern of pure MoS_2 only demonstrate the peaks for its hexagonal phase planes (Zhong et al., 2019; Iqbal et al., 2020). Scherer's formula is used to compute the crystalline size of the manufactured MoS_2 nanostructures.

$$D = \frac{K\lambda}{\beta \times cos\theta} \tag{1}$$

where β corresponds to FWHM value and θ represents angle of diffraction.

Raman spectroscopy is an effective tool that can detect material thickness, crystallographic orientation and phase transition. The comparative Raman spectra of as-grown MoS_2 nanorods and Pd-MoS_2 ((1 wt% & 2 wt%) are shown in Fig. 1b. The pure MoS_2 nanorods display two distinct Raman peaks, the E^1_{2g} mode at 379 cm^{-1} and the A_{1g} mode at 410 cm^{-1}, as shown in the figure. These findings are in agreement with previous studies (Late et al., 2014). The deposition of Pd atoms in nanorods causes an apparent red shift of around 4.0 cm^{-1} of the A_{1g} peak, whereas the position of the E^1_{2g} peak nearly remains unchanged. As a consequence, the difference (Δ) between both the E^1_{2g} and A_{1g} peaks in pure MoS_2 nanorods drops from 31.0 to 27.0 cm^{-1} in Pd-MoS_2 nanorods (1 wt% & 2 wt%) (Lin et al., 2014). As a result, this demonstrates that Pd doping can produce a considerable modification in the electronic structure of MoS_2 nanorods. Furthermore, the two new weak peaks found in Raman spectra of Pd-MoS_2 (1 wt% & 2 wt%) at 222 cm^{-1} and 33.8 cm^{-1}, which are coincided with the 1T phase molybdenum disulfide, could be attributed to modifications in the material's structure. The weak peak at 283 cm^{-1} belong to E_{1g} ([33]).

In Fig. 2, SEM and TEM micrographs were used to examine the microstructure and morphology of MoS_2 nanorods and

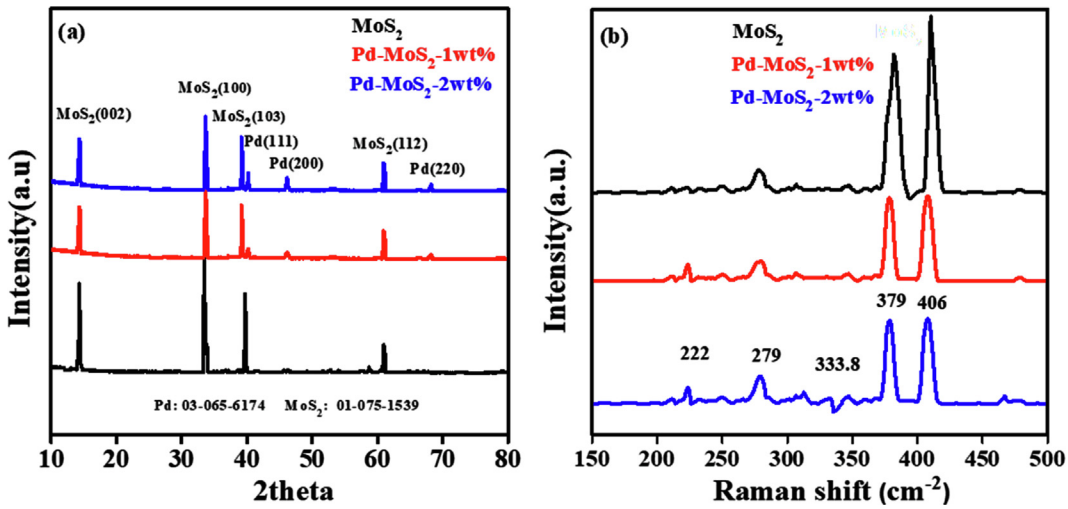

Fig. 1 **(a)** XRD pattern of MoS_2, Pd-MoS_2 (1 wt% &2 wt%), **(b)**. Raman spectra of MoS_2, Pd-MoS_2 (1 wt% & 2 wt%).

Pd-MoS_2. SEM and TEM images of pure MoS_2 nanorods revealed rod-like morphology, as illustrated in Fig. 2a and 2d. The numerous tiny Pd NPs distributed over the substrate on MoS_2 nanorods for Pd-MoS_2 (1 wt%) are clearly visible in SEM and TEM micrographs (Fig. 2b and e). More intriguingly, as demonstrated in transmission electron microscopy (TEM) image Fig. 2f, apparent Pd particles were regularly produced on the MoS_2 nanorods. Micrographs of the Pd-MoS_2 (2 wt%) nanorods using scanning electron microscopy (Fig. 2c) and transmission electron microscopy (Fig. 2f) reveal that Pd particles are uniformly adorned on the surfaces, as seen in the images encircled. The characteristic XPS spectrum of Pd-MoS_2 nanorods is shown in Fig. 3a, demonstrating the coexistence of Pd, Mo, and S. Pd element binding energies in the Pd doped MoS_2 nanorods are shown in Fig. 3b. Two distinctive peaks at 337.3 eV and 343.0 eV are attributed to Pd $3d_{5/2}$ and $3d_{3/2}$, correspondingly. The binding energies are substantially higher than those of Pd metals, and they are strikingly similar to those of Pd^{4+} (Yuwen et al., 2014; Hao et al., 2015). This implies that Mo atoms have been successfully replaced by Pd dopants, and that the Pd atoms have been covalently stabilized inside the lattice. Fig. 3c and d typically demonstrate high resolution XPS spectra of Mo 3d and S 2p. The binding energies of Mo and S for the MoS_2 nanorods without Pd doping are depicted in black curves. The Mo $3d_{5/2}$ and Mo $3d_{3/2}$ orbitals are ascribed to the peaks at 229.2 and 232.6 eV, correspondingly. When compared to the pure MoS_2 nanorods, the fundamental peaks of Mo in the Pd-MoS_2 nanorods reveal a smooth change toward lower binding energies, as seen in the figure. This shift could be explained by a decrease in Fermi level (EF) as a result of p type doping, as previously seen in other research (McDonnell et al., 2014). The

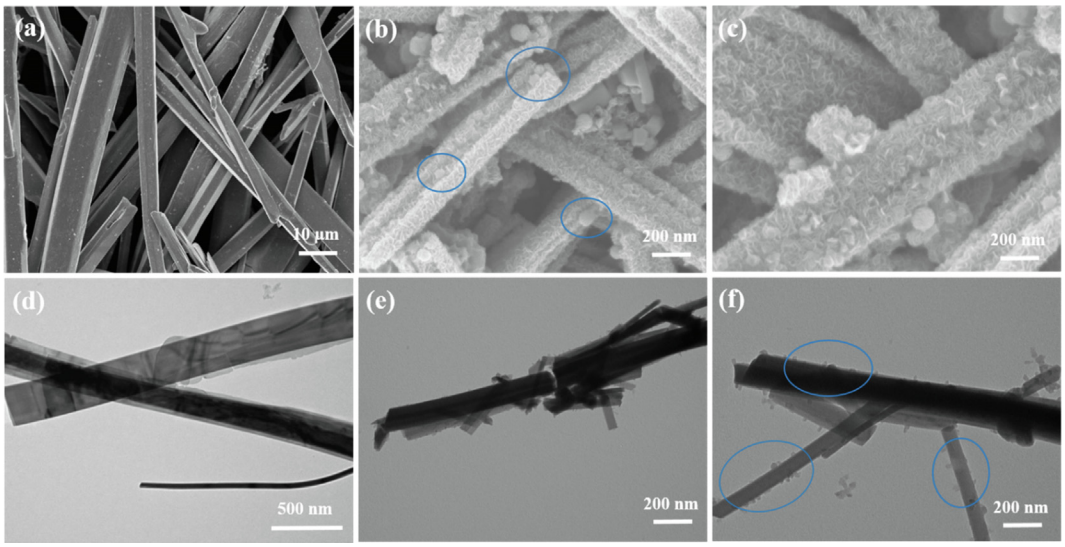

Fig. 2 **(a)** SEM image of MoS_2 nanorods **(b &c)** SEM images of Pd-MoS_2 (1 wt% & 2 wt%), **(d)** TEM image of MoS_2 **(e, f)** TEM image of Pd-MoS_2 (1 wt% & 2 wt%).

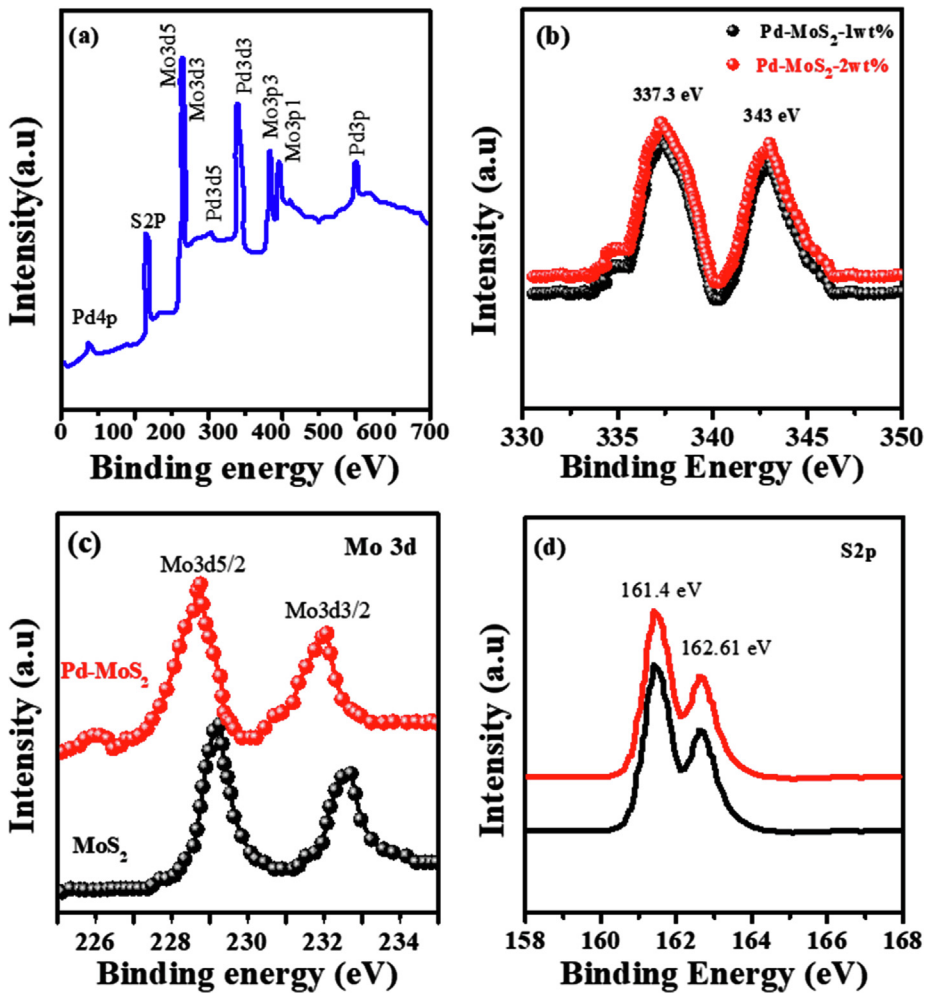

Fig. 3 **(a)** XPS survey scan of Pd-MoS_2 nanorods, **(b)** Pd 3d **(c)** Mo 3d (black for MoS_2 nanotube and red for Pd-MoS_2 2 wt%), **(d)** S2p (black for MoS_2 nanotube and red for Pd-MoS_2 2 wt%).

binding energies of the S $2p_{1/2}$ and S $2p_{3/2}$ emerge at 163.5 and 162.2 eV, correspondingly, and there is essentially no change between the nanorods with and without Pd doping.

The HER catalytic behavior of MoS_2 and Pd-MoS_2 was investigated using the demonstrative linear sweep voltammograms (LSVs) shown in Fig. 4a. The electrode with pure MoS_2 exhibited the lowest catalytic activity in acidic medium, which can be seen in Fig. 4a. Both the 1 wt% and 2 wt% Pd-MoS_2 samples displayed increased catalytic activity and lower overpotential when compared to pristine MoS_2. Initially, the pristine MoS_2 had a current density of 100 mA/cm_2 at 273 mV, which was analogous to prior MoS_2/rGO/NiS observations (Guangsheng et al., 2021). Secondly, 1 Wt% Pd doping on MoS_2 (η@100 mA cm^{-2} = 137 mV) further improve the activity. Further, Pd doping led to a dramatic improvement in catalytic performance toward the HER, which considerably outperforms 1% Pd-MoS_2 and pure MoS_2 catalysts. The 2 Wt% Pd–MoS_2 catalyst displayed a current density of 100 mA/cm^2 at an overpotential of only 119 mV, which is significantly better than that of hetero-structured tungsten-based catalysts (Jinsong et al., 2022). This is the best performance ever for heteroatom-doped MoS_2-based catalysts in acidic media (Zhilong et al., 2020; Luozhen et al., 2018; Sun et al., 2018). Tafel slope is key descriptor to evaluate the kinetics of HER. The Tafel slope was used to assess the kinetic behaviour of the Pd-MoS_2 nanorods for HER. As shown in Fig. 4b, the Tafel slope of 2 Wt% Pd-MoS_2 nanorods is 48 mV/dec, which is lower than 1 Wt% Pd-MoS_2 (70MmV/dec), MoS_2 nanorods (112 mV/dec) and the majority of previously described MoS_2-based HER electrocatalysts implying that Pd-MoS_2 nanorods has better reaction kinetics in the HER process (Zheng et al., 2018; Meng, 2020). The Tafel slope indicated a gradual drop from 112 mV/dec to 70–48 mV/dec, demonstrating that these materials have HER kinetics based upon Heyrovsky reaction, which is the rate-determining step in electrochemical desorption (Jung et al., 2017; Jue et al., 2019).

Moreover, Electrochemical impedance spectroscopy (EIS) measurements at −350 mV vs reversible hydrogen electrode (RHE) from 100 kHz to 0.1 Hz were performed to better investigate electrode kinetics during the HER process. Fig. 4c illustrates the Nyquist plots of these electrodes and the fitted equivalent circuit in the inset. The smaller and larger semicircles indicate the electrode–electrolyte interface resistance and the charge transfer resistance (Rct) of the H^+ reaction, respectively (Luo et al., 2018). As demonstrated in Fig. 4c, when compared to pure MoS_2 nanorods, the charge-transfer

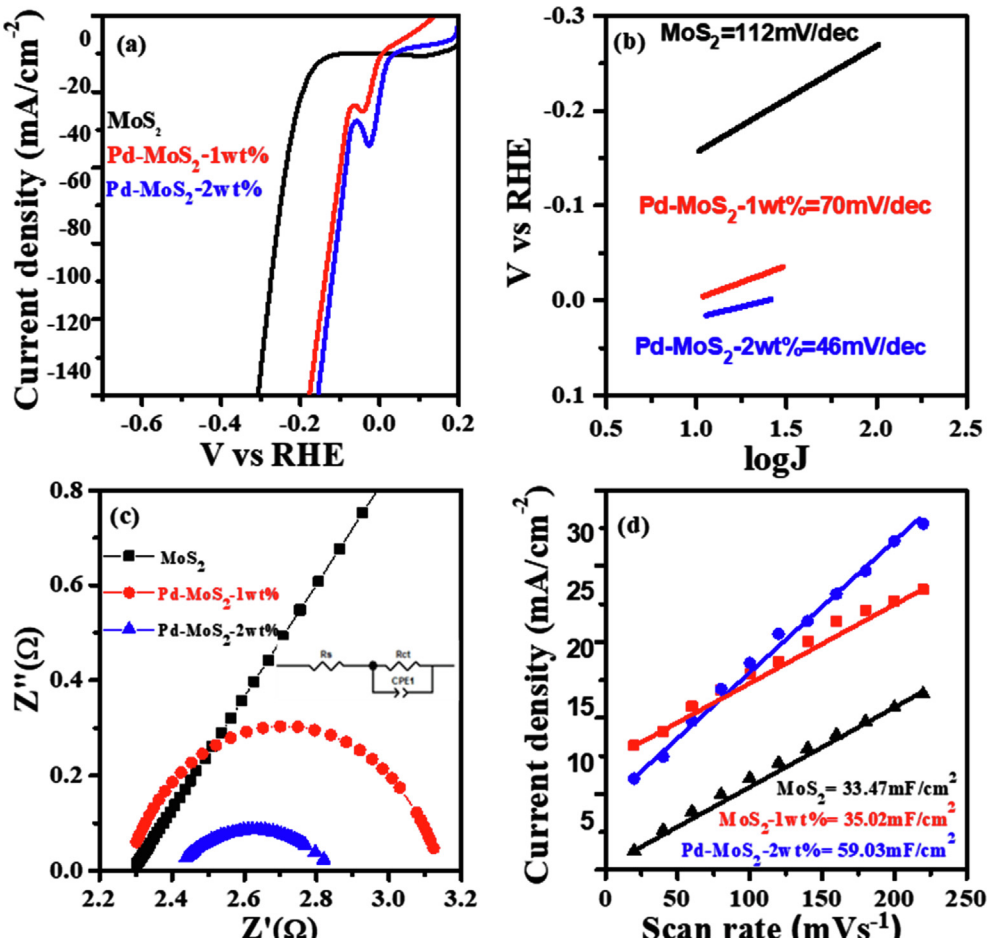

Fig. 4 **(a)** Polarization curves of pure MoS_2 nanorods, Pd-MoS_2 (1 wt% & 2 wt%), **(b)** Tafel slopes **(c)** Nyquist plot **(d)** Double layer capacitance recorded in non-faradic area of successive LSVs.

resistances drop significantly, with 1 Wt% Pd-MoS_2 (1.05) and 2 Wt% Pd-MoS_2 (0.4) having the lowest R_{ct} values. These findings suggest that a significant concentration of Pd doping can greatly enhance conductivity and charge transfer, hence boosting reaction efficiency. To gain a better understanding of these electrocatalysts, the electrochemical surface area (ECSA) values were examined. The electrochemical double layer capacitances (Cdl) were calculated using conventional CV, and the typical CV curves recorded for the different catalyst with variable scan rates are presented in Fig d (Fengming et al., 2021; Li et al., 2020; Miguel et al., 2015). In this scenario, a greater C_{dl} value indicates a higher ECSA. The Cdl of the 2 Wt% Pd-MoS_2 catalyst was approximately 59.03 mF cm^2, substantially higher than that of the 1 Wt% Pd-MoS_2 (35.02 mF cm^2) and pure MoS_2 (33.47 mF cm^{-2} as indicated in Fig. 4d. This result underpinned the effective synthesis of the Pd-MoS_2 catalyst, in which the 2Wt% doping of Pd on MoS_2 nanorods exposed more active sites 1 Wt% Pd-MoS_2 and pure MoS_2 nanorods. The Pd doped MoS_2 catalyst's HER performance was improved as a result of its efficient surface charge transfer, faster reaction rate, and large ECSA.

We are concerned about the catalyst's electrochemical stability because the hydrogen generating process could result in structural deformation and activity loss with continuous cycling (Ying et al., 2021; Zhijuan et al., November 2021). The electrocatalytic stability of Pd-MoS_2 nanorods was investigated by comparing LSV curves before and after cyclic voltammetry test (1000 cycle and even 3000 cycles for 2 wt% Pd-MoS_2) in 0.5 M H_2SO_4 solution. After 3000 cycles, the polarization curve shows no apparent change, as illustrated in Fig. 5c. Under the same experimental conditions, however, the HER stability of the pure MoS_2 nanorods as well as 1 wt% Pd-MoS_2 electrocatalysts (after 1000Cv cycles) is relatively poor. In electrocatalysis, durability is essential since the commercial electrode would have to be able to maintain a constant current for an extended period of time. To assess the durability, galvanostatic measurements were taken at potential of −0.4 V and the result (Fig. 5d) demonstrated that Pd-MoS_2 operated well after 10 h of continuous operation.

5. Conclusions

In conclusion, using a facile solvo-thermal route, we were able to successfully fabricate Pd-MoS_2 electrocatalyst with precise composition (doping) and morphologies (nanoparticles on nanorods). Ultimately, we discovered a catalyst for the HER in acidic conditions that has superior catalytic activity, increased conductivity, high surface area, and long-term durability. This research could pave the way for more logical design of cost-effective and high-performance hydrogen evolution catalysts.

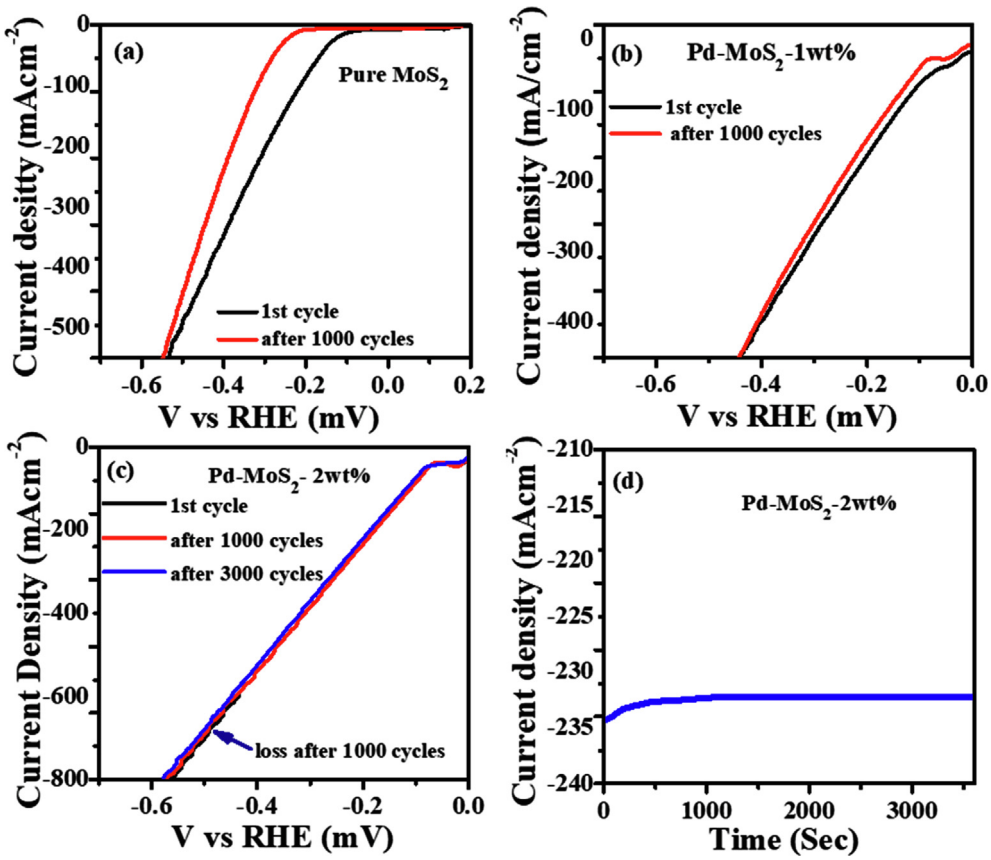

Fig. 5 **(a)** Stability tests for the first LSV curve and one after 1000 CV cycles for MoS_2 nanorodes **(b, c)** Pd-MoS_2 (1 wt% and 2 wt% (upto 3000 Cv cycles)) **(d)** Time dependent i-t curves at −0.4 V.

Acknowledgement

1. This work was financially supported by the National Natural Science of china (Nos. and) and Anhui Provincial Natural Science (No.).
2. Taif University Researchers Supporting Project number (TURSP-2020/241) Taif University, Taif Saudi Arabia.

References

Baohua, Z., Yiguo, X., Anning, J., Zhimin, X., Zhonghao, L., Jingcheng, H., 2017. Ionic liquid as reaction medium for synthesis of hierarchically structured one-dimensional MoO2 for efficient hydrogen evolution. ACS Appl. Mater. Interfaces 9 (8), 7217–7223.

Fengming, C., Liling, L., Yang, Z., Dongyang, L., Jinsong, Z., Fang, Y., Haiqing, Z., 2021. Large-current-stable bifunctional nanoporous Ferich nitride electrocatalysts for highly efficient overall water and urea splitting†. J. Mater. Chem. A 9, 10199.

Geng, X. et al, 2016. Pure and stable metallic phase molybdenum disulfide nanosheets for hydrogen evolution reaction. Nat. Commun. 7, 10672.

Guangsheng, L., Kunyapat, T., Xuefeng, L., Wenting, C., Tingjun, L., Shipeng, T., Minli, Z., Yu, C., Nannan, W., Yanqiu, Z., 2021. Defect-rich heterogeneous MoS_2/rGO/NiS nanocomposite for efficient pH-universal hydrogen evolution. Nanomaterials 11, 662.

L. Z. Hao, W. Gao,b Y. J. Liu, Y. M. Liu, Z. D. Han, Q. Z. Xue and J. Zhuc, Self-Powered Broadband, High-Detectivity and Ultrafast Photodetectors Based on Pd-MoS2/Si Heterojunctions, *Phys. Chem. Chem. Phys*., 00, 1-3 (2015).

Hinnemann, B. et al, 2005. Biornimetic hydrogen evolution: MoS_2 nanoparticles as catalyst for hydrogen evolution. J. Am. Chem. Soc. 127, 5308–5309.

Iqbal, T., Saleem, M., Riaz, S., et al, 2020. Comparison of optical constants of sputtered MoS_2 and MoS_2/Al_2O_3 composite thin films. J. Mater. Sci.: Mater. Electron. 31, 7753–7759.

Jaramillo, T.F. et al, 2007. Identification of active edge sites for electrochemical H2 evolution from MoS2 nanocatalysts. Science 317, 100–102.

Jingying, S., Fei, T., Fang, Y., Ze, Y., Bo, Y., Shuo, C., Zhifeng, R., Haiqing, Z., 2020. Robust hydrogen-evolving electrocatalyst from heterogeneous molybdenum disulfide-based catalyst. ACS Catal. 10, 1511–1519.

Jinsong, Z., Long, Z., Qian, Z., Liling, L., Ying, Q., Haiqing, Z., Dongyang, L., Fengming, C., Hui, W., Dongsheng, T.F., 2022. Boosting alkaline hydrogen and oxygen evolution kinetic process of tungsten disulfide-based heterostructures by multi-site engineering. Boosting Alkaline Hydrogen and Oxygen Evolution Kinetic Process of Tungsten Disulfide-Based Heterostructures by Multi-Site Engineering. 18 (1), 2104624.

Jue, H., Chengxu, Z., Peng, Y., Jingyi, X., Tao, D., Liu, Z., Bolong, H., Michael, K.H.L., Shihe, Y., 2019. Kinetic-oriented construction of MoS_2 synergistic interface to boost pH-universal hydrogen evolution. Adv. Funct. Mater. 30 (6), 1908520.

Jung, E.L., Jaemin, J., Taeg, Y.K., Sujin, K., Seong-I, K., Junghyo, N., Sunmin, R., Ki, T.N., Min, H.L., 2017. Catalytic synergy effect of MoS_2/reduced graphene oxide hybrids for a highly efficient hydrogen evolution reaction. RSC Adv. 7, 5480.

Kan, M. et al, 2014. Structures and phase transition of a MoS_2 monolayer. J. Phys. Chem. C 118, 1515–1522.

Karunadasa, H.I. et al, 2012. A molecular MoS_2 edge site mimic for catalytic hydrogen generation. Science 335, 698–702.

Kibsgaard, J., Chen, Z., Reinecke, B.N., Jaramillo, T.F., 2012. Engineering the surface structure of MoS_2 to preferentially expose active edge sites for electrocatalysis. Nat. Mater. 11, 963–969.

Late, D.J., Shaikh, P.A., Khare, R., Kashid, R.V., Chaudhary, M., More, M.A., Ogale, S.B., 2014. Pulsed laser-deposited MoS_2 thin films on W and Si: field emission and photoresponse studies. ACS Appl. Mater. Interfaces 6, 15881.

Li, H. et al, 2015. Optoelectronic crystal of artificial atoms in strain-textured molybdenum disulphide. Nat. Commun. 6, 7381.

Li, D.Y., Liao, L.L., Zhou, H.Q., Zhao, Y., Cai, F.M., Zeng, J.S., Liu, F., Wu, H., Tang, D.S., Yu, F., 2020. Highly active non-noble electrocatalyst from Co_2P/Ni_2P nanohybrids for pH-universal hydrogen evolution reaction. Mater. Today Phys. 16, 100314.

Liling, L., Lun, Y., Gang, Z., Haiqing, Z., Fengming, C., Yi, L., Xiuzhang, W., Fang, Y., 2019. Boosting pH-universal hydrogen evolution of molybdenum disulfide particles by interfacial engineering. Chin. J. Chem. 37, 288–294.

Liling, L., Jingying, S., Dongyang, L., Fang, Y., Yijun, Z., Yi, Y., Jinjian, W., Weichang, Z., Dongsheng, T., Shuo, C., Haiqing, Z., 2020. Highly robust non-noble alkaline hydrogen-evolving electrocatalyst from Se-doped molybdenum disulfide particles on interwoven $CoSe_2$ nanowire arrays. Small 16 (13), 1906629.

Lin, J.D., Han, C., Wang, F., Wang, R., Xiang, D., Qin, S., Zhang, X., Wang, L., Zhang, H., Wee, A.T.S., Chen, W., 2014. Electron-doping-enhanced trion formation in monolayer molybdenum disulfide functionalized with cesium carbonate. ACS Nano 8, 5323.

Longfei, W., Hofmann, Jan P., 2021. Comparing the Intrinsic HER Activity of Transition Metal Dichalcogenides: Pitfalls and Suggestions ACS Energy Lett. 6 (2021) 2619–2625.

Lukowski, M.A. et al, 2013. Enhanced hydrogen evolution catalysis from chemically exfoliated metallic MoS_2 nanosheets. J. Am. Chem. Soc. 135, 10274–10277.

Luo, Z., Ouyang, Y., Zhang, H., Xiao, M., Ge, J., Jiang, Z., Wang, J., Tang, D., Cao, X., Liu, C., Xing, W., 2018. Chemically activating MoS_2 via spontaneous atomic palladium interfacial doping towards efficient hydrogen evolution. Nat. Commun. 9, 2120.

Luozhen, B., Wei, G., Jiamin, S., Mingming, H., Fulin, L., Zhaofeng, G., Lei, S., Ning, H., Zai-xia, Y., Aimin, S., Yongquan, Q., Johnny, C.H., 2018. Phosphorus doped MoS_2 nanosheets supported on carbon cloths as efficient hydrogen generation electrocatalysts, Chem. Cat. Chem. 10, 1571-1577 (2018).

Ma, C.B. et al, 2014. MoS_2 nanoflower-decorated reduced graphene oxide paper for high-performance hydrogen evolution reaction. Nanoscale 6, 5624–5629.

McDonnell, S., Addou, R., Buie, C., Wallace, R.M., Hinkle, C.L., 2014. Defect-dominated doping and contact resistance in MoS_2. ACS NANO 8, 2880.

Meng, C. et al, 2020. Recent modification strategies of MoS_2 for enhanced electrocatalytic hydrogen evolution. Molecules 25, 1136.

Miguel, C.-A., Michael, L.S., Schmidt, J.R., Thomas, J.G., Ding, Q., Hung-C, C., Meng, L.T., Jr-Hau, H., Song, J., 2015. Efficient hydrogen evolution catalysis using ternary pyrite-type cobalt phosphosulphide. Nature. Mater. 14 (12), 1245–1251.

Peng, Q., Qi, X., Gong, X., Chen, Y., 2021. 1T-MoS_2 coordinated bimetal atoms as active centers to facilitate hydrogen generation. Materials 14, 4073.

Santra, S., Hota, P.K., Bhattacharyya, R., Bera, P., Ghosh, P., Mandal, S.K., 2013. Palladium Nanoparticles on graphite oxide: a recyclable catalyst for the synthesis of biaryl cores. ACS Catal. 3, 2776–2789.

Seh, Z.W., Kibsgaard, J., Dickens, C.F., Chorkendorff, I., Nørskov, J. K., Jaramillo, T.F., 2017. Combining theory and experiment in electrocatalysis: Insights into materials design. Science 355 eaad4998.

Song, X., Li, B., Peng, W., Wang, C., Li, K., Zhu, Y., Mei, Y.i., 2021. A palladium doped 1T-phase molybdenum disulfide-black phosphorene two-dimensional van der Waals heterostructure for visible-light enhanced electrocatalytic hydrogen evolution. Nanoscale 13, 5892–5900.

Sun, K., Liu, Y., Pan, Y., Zhu, H., Zhao, J., Zeng, L., Liu, Z., Liu, C., 2018. Targeted bottom-up synthesis of 1T-phase MoS_2 arrays with high electrocatalytic hydrogen evolution activity by simultaneous structure and morphology engineering. Nano Res. 11, 4368–4379.

Tsai, C. et al, 2017. Electrochemical generation of sulfur vacancies in the basal plane of MoS2 for hydrogen evolution. Nat. Commun. 8, 15113.

Voiry, D. et al, 2016. The role of electronic coupling between substrate and 2D MoS_2 nanosheets in electrocatalytic production of hydrogen. Nat. Mater. 15, 1003–1009.

Wu, W., Niu, C., Wei, C., Jia, Y., Li, C., Xu, Q., 2019. Activation of MoS2 Basal planes for hydrogen evolution by zinc. Angew. Chem., Int. Ed. 58, 1–6.

Yan, Y., Xia, B., Xu, Z., Wang, X., 2014. Recent development of molybdenum sulfides as advanced electrocatalysts for hydrogen evolution reaction. ACS Catalysis 4, 1693–1705.

Yang, J. et al, 2016. Porous molybdenum phosphide nano-octahedrons derived from confined phosphorization in UIO-66 for efficient hydrogen evolution. Angew. Chem. Int. Ed. 55, 12854.

Ying, Z., Yuxiao, G., Zhi, C., Zhenjiang, L., Tianyi, M., Zexing, W., Lei, W., 2021. Trifle Pt coupled with NiFe hydroxide synthesized via corrosion engineering to boost the cleavage of water molecule for alkaline water-splitting. Appl. Catal. B 297, 120395.

Yipeng, Z., Shuwen, N., Yishang, W., Xusheng, Z., Jinyan, C., Jian, Y., Yufang, X., Yun, L., Jianbin, Z., Junfa, Z., Xiaojing, L., Gongming, W., Yitai, Q., 2019. Tuning orbital orientation endows molybdenum disulfide with exceptional alkaline hydrogen evolution capability. Nat. Commun. 10, 1217.

Yixin Yao, Kelong Ao, Pengfei Lv and Qufu Wei, MoS_2 Coexisting in 1T and 2H Phases Synthesized by Common Hydrothermal Method for Hydrogen Evolution Reaction, *Nanomaterials (Basel)* 9, 844 (2019).

Yuwen, L., Xu, F., Xue, B., Luo, Z., Zhang, Q., Bao, B., Su, S., Weng, L., Huang, W., Wang, L., 2014. General synthesis of noble metal (Au, Ag, Pd, Pt) nanocrystal modified MoS2 nanosheets and the enhanced catalytic activity of Pd–MoS2 for methanol oxidation. Nanoscale 6, 5762.

Zexing, W., Dazong, N., Min, S., Tiantian, J., Gengtao, F., Xien, L., 2012. Facile synthesis of Co-Fe-B-P nanochains as efficient bifunctional electrocatalysts for overall water-splitting. Nanoscale 00, 1–3.

Zexing, W., Ying, Z., Wei, J., Baohua, J., Jie, W., Tianyi, M., 2020. Recent progress of vacancy engineering for electrochemical energy conversion related applications. Adv. Funct. Mater. 31 (9), 2009070.

Zexing, W., Ying, Z., Hengbo, W., Yuxiao, G., Zhi, C., Wei, J., Jinsong, W., Tianyi, M., 2021. Corrosion Engineering on iron foam toward efficiently electrocatalytic overall water splitting powered by sustainable energy. Adv. Funct. Mater. 31, 2010437.

Zheng, Y., Jiao, Y., Jaroniec, M., Qiao, S.Z., 2015. Advancing the electrochemistry of the hydrogen-evolution reaction through combining experiment and theory. Angew. Chem., Int. Ed. 54, 52–65.

Zheng, Y., Jiao, Y., Vasileff, A., Qiao, S.Z., 2018. The hydrogen evolution reaction in alkaline solution: from theory, single crystal models, to practical electrocatalysts. Angew. Chem., Int. Ed. 57, 7568–7579.

Zhijuan, L., Xiaodong, W., Xian, J., Binbin, S., Zhishun, T., Dongmei, S., Gengtao, F., Yawen, T., November 2021. Surface carbon layer controllable Ni_3Fe particles confined in hierarchical N-doped carbon framework boosting oxygen evolution reaction. Adv. Powd. Mater. 23. https://doi.org/10.1016/j.apmate.2021.11.007.

Zhilong, Z., Liang, Y., Meng, G., Xiya, C., Wu, Z., Chao, M., Lihui, W., Junfa, Z., Xiangyu, M., Jingting, H., Yunchuan, T., Sisi, W.,

Jun, Zhongqun, T., Dehui, D., . Boosting hydrogen evolution on MoS_2 via co-confining selenium in surface and cobalt in inner layer. Nat Commun 11, 3315.

Zhong, Y., Shi, T., Huang, Y., et al, 2019. Three-dimensional MoS_2/-graphene aerogel as binder-free electrode for Li-ion battery. Nanoscale Res. Lett. 14, 85.